Chemistry and electrical properties of surfaces of GaN and GaN/AlGaN heterostructures

Tamotsu Hashizume,[a] Shinya Ootomo, Susumu Oyama, Masanobu Konishi, and Hideki Hasegawa
Research Center for Integrated Quantum Electronics (RCIQE), Hokkaido University, Sapporo, 060-8628, Japan

(Received 9 January 2001; accepted 7 May 2001)

Chemical and electrical properties of the surfaces of GaN and GaN/AlGaN heterostructures were systematically investigated by x-ray photoelectron spectroscopy (XPS), capacitance–voltage, and current–voltage measurements. From *in situ* XPS study, relatively smaller band bending of 0.6 eV was seen at the GaN (2×2) surface grown by radio frequency-assisted molecular beam epitaxy on the metalorganic vapor phase epitaxy GaN template. After exposing the sample surface to air, strong band bending took place at the surface. The surface treatment in NH_4OH solution and N_2 plasma was found to reduce the surface Fermi level pinning. Surface passivation process of GaN utilizing SiN_x film by electron-cyclotron-resonance assisted plasma chemical vapor deposition (ECR–CVD) achieved low interface state density, $2\times10^{11}\mathrm{cm}^{-2}\,\mathrm{eV}^{-1}$. No pronounced stress remained at the SiN_x/GaN interface, which was confirmed by Raman spectroscopy. The present NH_4OH/ECR–N_2 plasma treatment was also found to be effective in realizing well-ordered and nearly oxide-free surface of a GaN/AlGaN heterostructure. The subsequent passivation process using the ECR–CVD SiN_x film enhanced the drain current in the gateless GaN/AlGaN high electron mobility transistor. A surface passivation process utilizing an ultrathin Al-oxide layer reduced leakage current and improved gate controllability of two-dimensional electron gas in the Schottky gate contact fabricated on the GaN/AlGaN heterostructures. © *2001 American Vacuum Society.*
[DOI: 10.1116/1.1383078]

I. INTRODUCTION

GaN and related heterostructures are now well established as materials for the production of high-power/high-frequency devices such as high-electron mobility transistors (HEMTs) and heterojunction bipolar transistors. These are key devices for the next-generation wireless communication systems, e.g., International Mobile Telecommunications-2000 (IMT-2000), with ultrahigh speed and large-volume performance. Reproducibility of the device fabrication process and reliability of the device operation are indispensable for realization of high-performance wireless systems. In fact, surface-trap related effects have been reported very recently for GaN/AlGaN HEMT devices, namely a significant frequency-dependent collapse or the so-called ''direct current (dc)-to-radio frequency (rf) dispersion'' in drain current.[1,2] Due to the high doping and the degradation of the crystalline quality of an AlGaN layer with a relatively higher Al content, poor Schottky contact properties, especially large leakage current, were often observed in GaN/AlGaN HEMT devices. This significantly affects the noise performance of HEMT devices.[3] Thus, understanding and controlling surface properties of GaN and GaN-based heterostructures is of the utmost importance for their reliable performance with successful surface passivation.

Chemical and electronic properties of clean GaN surfaces and metal/GaN interfaces processed in an ultrahigh vacuum (UHV) environment have been investigated by several groups.[4–6] However, there are a few reports on the processed GaN surfaces such as chemically treated surfaces, plasma-treated surfaces, etc., and on the surfaces of GaN/AlGaN heterostructures, in spite of the fact that the understanding of these surfaces is necessary for the development of actual device fabrication process. For the final stage of surface passivation, the use of thick insulating films is indispensable. In this regard, several studies on insulator-semiconductor (IS) structures using GaN have been performed. Pioneering works on the GaN IS structures using deposited insulating films were reported by Casey *et al.*[7] and Sawada *et al.*[8] Therrien *et al.*[9] reported a remote plasma process including separate plasma oxidation of GaN and deposition of thick SiO_2 film. Hong *et al.*[10] have very recently demonstrated the $Ga_2O_3(Gd_2O_3)$/GaN system with low interface state density. For the GaN/AlGaN structures, Green *et al.*[2] have demonstrated that the use of a Si_3N_4 passivation layer improved rf performance of a GaN/AlGaN HEMT, and Kahn and co-workers[11,12] recently reported the fabrication of the metal–oxide–semiconductor GaN/AlGaN HEMT and its potential of high dc and microwave performance. However, interface properties of GaN and AlGaN IS structures are not fully understood and surface passivation processes of GaN and GaN/AlGaN heterostructures are not well optimized. Furthermore, *in situ* characterization of epitaxially grown surfaces is desirable for improving optical and electronic properties of GaN-based heterointerfaces.

In this article, we present a systematic investigation on chemical and electrical properties of surfaces of GaN and

[a]Electronic mail: hashi@rciqe.hokudai.ac.jp

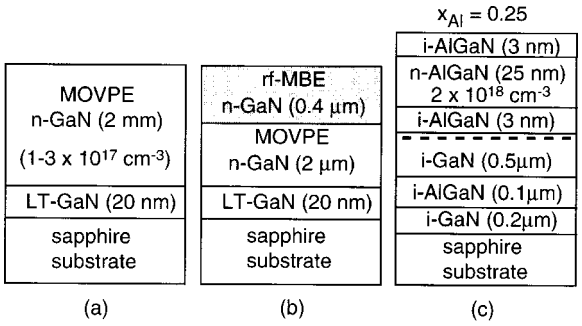

FIG. 1. Schematic illustrations of GaN and GaN/AlGaN sample structures: (a) MOVPE *n*-GaN, (b) rf-MBE *n*-GaN, and (c) MOVPE GaN/AlGaN heterostructure.

GaN/AlGaN heterostructures for the optimization of a surface passivation process. Homoepitaxial GaN (2×2) surface grown by molecular beam epitaxy (MBE), chemically treated surface, and plasma treated surface were characterized by x-ray photoelectron spectroscopy (XPS). Electrical properties of the surfaces of GaN and GaN/AlGaN heterostructures with surface passivation were evaluated by capacitance–voltage $(C-V)$ and current–voltage $(I-V)$ methods.

II. EXPERIMENT

A. GaN and GaN/AlGaN sample structures

Figure 1 shows schematic illustrations of GaN and GaN/AlGaN sample structures. High-quality epitaxial GaN wafers grown by metalorganic vapor phase epitaxy (MOVPE) were supplied by Hitachi Cable Ltd. A buffer GaN layer (LT–GaN) was grown on a sapphire substrate at low temperatures (500–550 °C) followed by the growth of Si-doped GaN layer at 1000 °C. Typical values of electron concentration and mobility of the Si-doped layer at room temperature (RT) is $2\times10^{17}\,\mathrm{cm}^{-3}$ and $500\,\mathrm{cm}^2/\mathrm{V\,s}$, respectively.

As a clean reference GaN surface, a homoepitaxial GaN layer was grown by the rf-radical assisted molecular beam epitaxy (rf–MBE) on MOVPE GaN template, as shown in Fig. 1(b). The substrate temperature was 650 °C. The nitrogen radical beam was produced with rf power of 200 W and nitrogen gas flow ratio of 2.5 sccm (corresponding to 5×10^{-5} Torr). The growth rate was about 0.1 μm/h. Streak reflection high-energy electron diffraction pattern with (2×2) reconstruction was maintained during the growth, indicating that the grown layer had the Ga-terminated surface.[13,14] The full width at half maximum of the x-ray rocking curve from the homoepitaxial GaN layer became the same as that of the MOVPE GaN.

The heterostructure sample consisting of GaN and $Al_{0.25}Ga_{0.75}N$ layers grown by MOVPE, as shown in Fig. 1(c), was also supplied by Hitachi Cable Ltd. Typical values of the electron concentration and mobility of the heterostructure sample at RT were $1.5\times10^{13}\,\mathrm{cm}^{-2}$ and $1300\,\mathrm{cm}^2/\mathrm{V\,s}$, respectively, comparable to those reported in the literature. In addition, the sample showed clear Shuvnikov–de Haas oscillation in magnetoresistance characteristics at 2 K, and the electron concentration determined from the Landau plots of the oscillation was in good agreement with the value obtained by the Hall measurement at the same temperature. These results clearly indicated the existence of two-dimensional electron gas (2DEG) at the GaN/AlGaN heterointerface.

B. Surface passivation process

In view of actual device fabrication process, a surface passivation process started from a simple wet treatment in organic solvents at RT and in an NH_4OH solution at 50 °C for 5–10 min. Then GaN and GaN/AlGaN surfaces were processed in electron-cyclotron-resonance (ECR) excited N_2 plasma at 300 °C for 1–5 min with microwave (2.75 GHz) power of 50 W. Final passivation was performed by the deposition of SiN_x film on the sample surface at 280 °C by ECR assisted plasma chemical vapor deposition (ECR–CVD) using SiH_4 and N_2. We obtained a diffractive index value of 1.98 for the deposited SiN_x film. Thickness of the deposited film ranged from 40 to 60 nm.

As an ohmic contact for $I-V$ and $C-V$ measurements, a Ti/Al/Ti/Au contact ring was deposited on the surfaces of GaN and GaN/AlGaN followed by the annealing at 600 °C for 2 min in N_2 ambient. The Pt/Au contact and the Al contact with a diameter of 500 μm were used for the Schottky and metal–insulater–semiconductor (MIS) structures, respectively.

C. Characterization methods

The surface chemical properties of GaN and GaN/AlGaN samples were characterized by XPS. The XPS measurement system (Perkin Elmer PHI 1600C) consists of a spherical capacitor analyzer and a monochromated Al $K\alpha$ x-ray source $(h\nu=1486.6\,\mathrm{eV})$. The XPS system is connected to the MBE growth chamber and ECR–CVD chamber through the UHV transfer system with a base pressure of 2×10^{-10} Torr, thereby *in situ* XPS characterization of the MBE-grown or plasma-processed surfaces is available. The binding energies of the spectra were carefully calibrated through separate measurements of Cu $2p_{3/2}$, Ag $3d_{5/2}$, and Au $4f_{7/2}$ peak positions. Atomic force microscope (AFM) observation of GaN surfaces after various types of surface treatments was carried out using a Nanoscope II (Digital Instruments). $C-V$ curves were measured at RT using a HP 4192A LF impedance analyzer. In order to avoid the impact of the series resistance of the epitaxial GaN and AlGaN layers on the $C-V$ measurements, characterization took place at a frequency of 100 kHz. $C-V$ curves were recorded at a sweep rate of 100 mV/s.

III. RESULTS AND DISCUSSION

A. XPS and AFM characterization of GaN surfaces

Figure 2 shows Ga $3d$ and N $1s$ *in situ* spectra obtained from the rf–MBE grown GaN (2×2) surface and *ex situ* spectra from the air-exposed surface. After exposing the

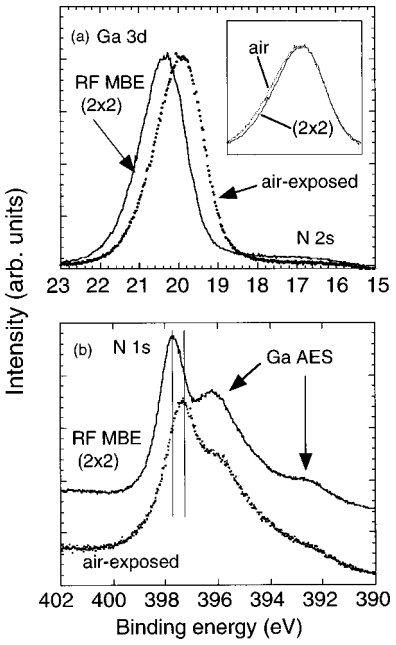

FIG. 2. XPS Ga 3*d* and N 1*s* *in situ* spectra obtained from the rf–MBE grown GaN (2×2) surface and *ex situ* spectra from the air-exposed surface.

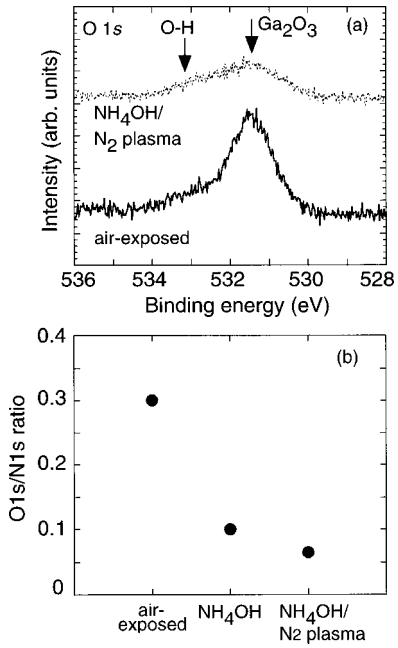

FIG. 3. (a) O 1*s* spectra of the MOVPE sample after the air exposure and the NH_4OH/N_2 plasma treatments, and (b) change in the XPS integrated intensity of the O 1*s* level normalized by the N 1*s* level.

sample to air, noticeable peak shift toward lower binding energies was seen in both Ga 3*d* and N 1*s* spectra. In addition, an asymmetric feature of the Ga 3*d* level with a shoulder at higher binding energies, as shown in the inset of Fig. 2(a), and the narrower energy separation between the N 1*s* and Ga Auger electron spectroscopy (AES) peaks [Fig. 2(b)] were observed at the air-exposed surface. This feature as well as a high intensity of the O 1*s* level indicated that an air-exposed GaN surface was covered with a natural oxide layer including a Ga-oxide component. The rigorous deconvolution of the Ga 3*d* and N 1*s* spectra led to the conclusion that the air-exposed surface exhibits Ga-rich phase and that Ga_2O_3 is the dominant component in the surface natural oxide.

Figure 3(a) shows the O 1*s* spectra of the MOVPE sample after the air exposure and the NH_4OH/N_2 plasma treatments. Two peaks corresponding to the O–H bond[15,16] and the Ga_2O_3 bond[17,18] appeared at the air-exposed surface. After the NH_4OH/N_2 plasma treatments, drastic reduction of the O 1*s* peak was observed. In addition, this process realized a shoulderless feature of the Ga 3*d* level and clear separation of energy peaks between the N 1*s* and Ga AES signals. The effect of the surface treatments on the reduction of natural oxide layer on the GaN surface was summarized in Fig. 3(b), in terms of change in the XPS integrated intensity of the O 1*s* level normalized by the N 1*s* level. As mentioned earlier, a high intensity of the O 1*s* peak appeared on the air-exposed surface. After the NH_4OH treatment, significant decrease of the oxide components was observed. Further reduction of oxide components was achieved by the surface treatment in the ECR–N_2 plasma. The plasma process was also effective in removing surface contamination. The Ga 3*d*/N 1*s* intensity ratio became close to the stoichiometric value after the series of surface passivation process. This is due to the removal of natural gallium oxide layer, which made the surface nearly oxide-free.

Figure 4 shows the positions of surface Fermi level (E_{fs}) for various GaN surfaces. The value of E_{fs} was determined by the peak position of the Ga 3*d* core level where the value of 17.8 eV corresponds to the separation between the Ga 3*d* level and the valence band maximum, E_v.[4,5,19,20] We confirmed that the E_{fs} positions estimated by the N 1*s* core level and the valence band spectra were identical to the results shown in Fig. 4. Note that the data for the N_2-plasma treated surface and SiN_x (2 nm)-deposited surfaces were obtained by *in situ* XPS measurements.

The fresh MBE-grown (2×2) surface showed E_{fs} to lie at 2.7 eV above E_v, indicating the upward band bending of 0.6 eV. It is well known that the nitrogen-ion bombardment or the Ga deposition followed by the UHV annealing

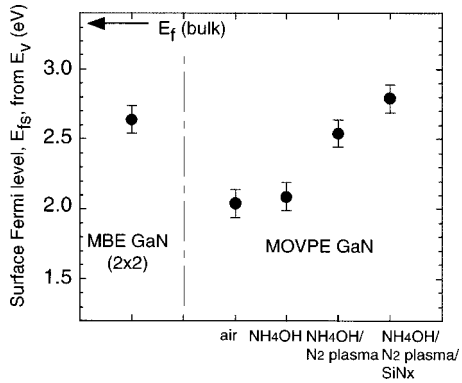

FIG. 4. Positions of surface Fermi level (E_{fs}) for various GaN surfaces.

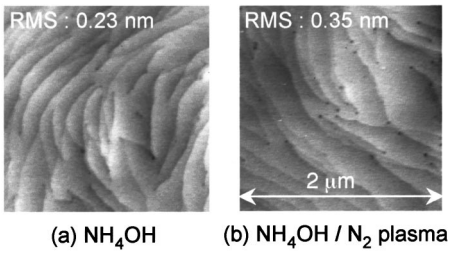

FIG. 5. AFM images of the GaN surfaces after the NH_4OH and ECR N_2-plasma treatments.

at 800–900 °C realized clean (1×1)-ordered GaN surfaces.[4,5,21] These clean (1×1) surfaces showed relatively strong band bending. Bermudez[4,6] and Wu and Kahn[5] concluded that the band bending of 0.8–0.9 eV existed at such (1×1) surfaces. Stronger bending of about 2.1 eV was reported by Dhesi and co-workers.[22] In comparison, our *in situ* XPS study showed smaller band bending on the MBE-grown (2×2) surface. Theoretical calculations[23,24] predicted that the (2×2) reconstruction is the most stable structure for the (0001) Ga-terminated surface.

The position of E_{fs} was found at $Ev+2.0$ eV for the air-exposed MOVPE GaN sample, indicating relatively strong band bending of 1.3–1.4 eV. Wu and Kahn[5] and Wolter *et al.*[25] reported similar E_{fs} position at the air-exposed MOVPE GaN surface. The surface included natural oxide and contamination, and showed a nonstoichiometric (Ga-rich) feature. This probably causes the strong band bending. The surface band bending is sensitive to contamination, disorder, and defects at the surface since the Fermi level position is governed by the balance between the surface charge and the ionized donors in the depletion region. In contrast to these results, Bermudez[4] concluded that smaller band bending of 0.4 eV appeared at the oxidized and contaminated GaN surface. The reason for the discrepancy is not clear yet.

After the surface treatment in the NH_4OH solution at 50 °C for 10 min, the surface natural oxide was reduced, as shown in Fig. 3. However, the E_{fs} position did not change from the position at the air-exposed surface. The following surface process in ECR-excited N_2 plasma was found to have an effect on the reduction of the surface band bending, as shown in Fig. 4. The E_{fs} position moved up to 0.4–0.5 eV above the position of the air-exposed sample. The depletion of N atoms was found at the air-exposed sample, leading to the vague separation of the N 1*s* and Ga AES levels, as seen in the bottom trace in Fig. 2(b). The Ga-to-N ratio was 1.12 at the air-exposed surface, consistent with the result of Wu and Kahn.[5] The ECR–N_2 plasma treatment seems to partially recover or terminate N-deficiency related defects. The subsequent deposition of SiN_x film by ECR–CVD realized further upward movement of surface Fermi level, indicating pronounced passivation effect.

Typical AFM images of the GaN surfaces after the NH_4OH and ECR N_2-plasma treatments were shown in Fig. 5. The as-grown MOVPE GaN exhibited smooth surface with a root-mean-square (rms) value of 0.23 nm. The NH_4OH treatment completely maintained the surface smoothness showing the characteristic feature dominated by monolayer steps. The rms value comparable to that of the as-grown sample was obtained even after the plasma treatment process, as shown in Fig. 5(b).

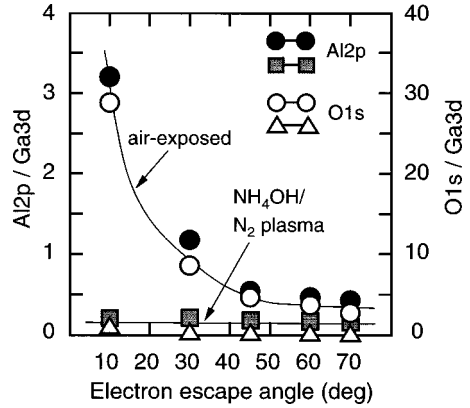

FIG. 6. Integrated XPS intensity ratios of Al 2*p*/Ga 3*d* and O 1*s*/Ga 3*d* obtained from the GaN/AlGaN heterostructure surface as a function of the electron escape angle.

B. XPS characterization of GaN/AlGaN surface

The air-exposed surface of the MOVPE GaN/AlGaN heterostructure sample exhibited highly nonstoichiometric phase with large amounts of natural oxide.[26] Figure 6 shows the integrated XPS intensity ratios of Al 2*p*/Ga 3*d* and O 1*s*/Ga 3*d* as a function of the electron escape angle. The air-exposed sample exhibited complicated composition distribution in depth. In particular, steep increase of Al 2*p* and O 1*s* intensities at shallower escape angles indicated that the Al-oxide component is dominant on the topmost surface. The Al 2*p* core-level exhibited broad spectra with a peak binding energy very close to that of Al_2O_3, and asymmetric spectra with a shoulder including the Ga_2O_3 component appeared in the Ga 3*d* core level.[26] Such a natural oxide layer can be removed after the NH_4OH/ECR–N_2 plasma treatments, as indicated by the shaded squares and open triangles in Fig. 6. A significant reduction of the O 1*s* intensity is seen, and the composition does not vary with depth from this surface. In fact, the surface treatment led to symmetric features in both Al 2*p* and Ga 3*d* spectra where the peak positions of these spectra were very close to those of the Al–N bond and the Ga–N bond. From the relative XPS sensitivity factors, the Al composition was calculated to be 0.23, in reasonably agreement with the value of 0.25 obtained from the separate x-ray diffraction measurement. Thus, the present NH_4OH/ECR–N_2 plasma treatment was found to be effective in realizing well ordered and nearly oxide-free surface of a GaN/AlGaN heterostructure.

In order to improve Schottky gate properties on the GaN/AlGaN HEMT structure, a passivation approach was attempted. The process started from the formation of ultrathin (1 nm) Al layer on the NH_4OH-treated GaN/AlGaN surface at RT using a *K* cell in the MBE chamber. Then the

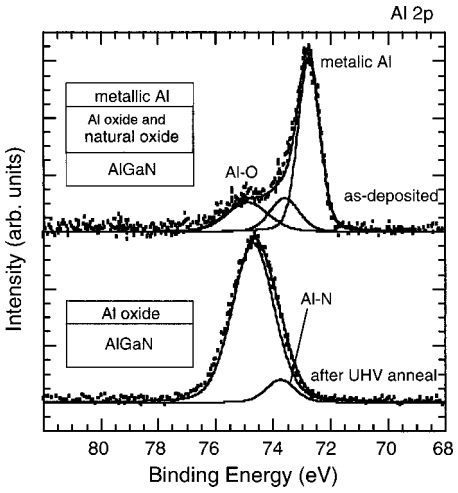

FIG. 7. *In situ* XPS Al $2p$ spectra of the NH_4OH-treated GaN/AlGaN/Al sample prepared in the MBE chamber (a) before and (b) after the UHV anneal at 700 °C for 10 min.

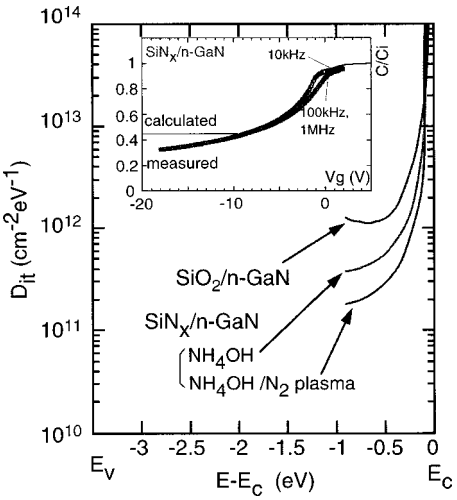

FIG. 8. Distributions of interface state density (D_{it}) of the fabricated n-GaN MIS structures. Typical $C-V$ data obtained from the NH_4OH/ECR–N_2 plasma passivated sample were plotted in the inset.

sample was annealed at 700 °C for 10 min in an UHV environment (base pressure: 2×10^{-10} Torr). The basic idea of this process is to convert the natural oxide on the AlGaN surface to the Al oxide (Al_2O_3) by use of the reduction reaction of natural oxide with active metallic Al driven by the large heat of formation of Al_2O_3.

Figure 7 shows *in situ* XPS Al $2p$ spectra of the NH_4OH-treated GaN/AlGaN/Al sample prepared in the MBE chamber. In spite of the fact that Al was evaporated at room temperature in an UHV environment, the Al $2p$ spectra clearly included an oxide component (Al_2O_3) in addition to the metallic Al and the Al–N bonds. Judging from the escape-angle dependence of the Al $2p$ and O $1s$ peak intensities (not shown here), an interfacial layer resulting from the reaction between Al and natural oxide was formed at the Al/AlGaN interface. Such a layer structure (Al+oxides) was found to convert to the Al_2O_3 layer completely after the UHV thermal annealing at 700 °C for 10 min, as shown in the bottom trace in Fig. 7. Note that the Al–N peak originated from the AlGaN layer underneath the topmost Al-oxide layer. Thus the present UHV process allows us to form the GaN/AlGaN/ultrathin Al oxide passivation structure.

C. Electrical properties of passivated GaN and GaN/AlGaN surfaces

Electrical properties of the passivated GaN surface were investigated using a MIS structure with a thick (40–60 nm) SiN_x film. Figure 8 shows distributions of interface state density (D_{it}) of the fabricated SiN_x/n-GaN structures. For comparison, the D_{it} distribution of the SiO_2/n-GaN interface was plotted. The D_{it} distributions were calculated by applying the Terman method to the measured $C-V$ curves at room temperature. Typical $C-V$ data of the SiN_x/n-GaN sample with the NH_4OH/ECR–N_2 plasma treatment were plotted in the inset of Fig. 8. Also shown is the calculated curve based on the accumulation, depletion and inversion behavior for the MIS structure. For calculation, an effective electron mass of $0.22\,m_0$, an effective hole mass of $0.8\,m_0$, a dielectric constant of 9.5 and an energy gap of 3.39 eV were used for GaN at room temperature.

In comparison with the SiO_2/n-GaN interface, the SiN_x/GaN structures showed relatively low density of interface states. The measured $C-V$ curves were very close to the calculated ones, and small hysteresis and frequency dispersion were achieved. Furthermore, clear deep depletion behavior was observed at room temperature, as shown in the inset of Fig. 8. This deep depletion feature with no inversion capacitance characteristics is typical of wide-gap semiconductor MIS structures such as SiO_2/SiC[27] and AlN/SiC,[28] because the generation rate of the minority carriers (holes) is extremely low at room temperature. The $1/C^2$ characteristics as a function of the applied gate voltage showed good linear behavior, indicating the presence of deep depletion by pronounced band bending. From the slope of the plots, the carrier density of n-GaN layer was determined to be $1.7\times10^{17}\,cm^{-3}$, very close to the value of $2.0\times10^{17}\,cm^{-3}$ obtained from the Hall measurement. These results indicated that the control of surface potential of GaN over a remarkably wide range was achieved in the SiN_x/GaN interface. As shown in Fig. 8, the NH_4OH/ECR–N_2 plasma passivation process achieved low D_{it} value of $2\times10^{11}\,cm^{-2}\,eV^{-1}$. These results were consistent with the reduction of the surface band bending at the passivated GaN surface, as confirmed by XPS analysis (Fig. 4). Furthermore, the Raman spectroscopy study revealed that no stress was found at the present SiN_x/GaN structure.

Based on these results, the present NH_4OH/ECR–N_2 plasma passivation followed by the deposition of thick SiN_x film was applied to the surface of GaN/AlGaN heterostructure. Figure 9 shows the $I-V$ characteristics of the gateless GaN/AlGaN HEMT structure with and without surface passivation. The drain to source distance is 8 μm. Enhancement of drain current was observed for the structure with the surface passivation. Similar effect on the drain current as well

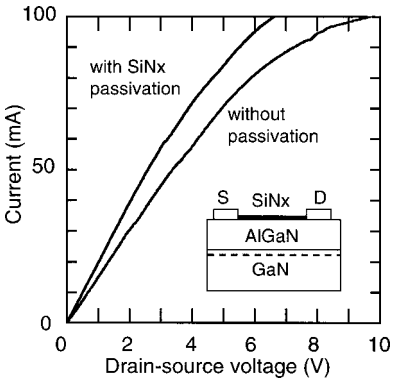

FIG. 9. $I-V$ characteristics of the gateless GaN/AlGaN HEMT structure with and without SiN_x surface passivation.

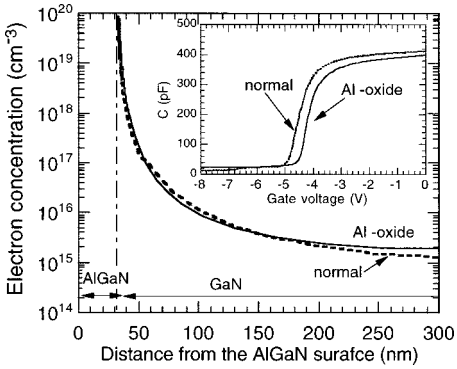

FIG. 11. Profiles of electron concentration near the GaN/AlGaN interface as a function of distance from the top AlGaN surface. The measured $C-V$ curves on the Pt/Au Schottky gates are shown in the inset.

as the rf characteristics were demonstrated in the GaN/AlGaN HEMT with the Si_3N_4 passivation layer.[2] Our detailed XPS study on GaN surface indicated that the reduction of surface band bending by passivation could enhance the 2DEG density at the GaN/AlGaN interface, and that the reduction of surface states could suppress surface-trap related effects.

Finally, a surface passivation approach, as described in Sec. III B, was attempted to improve Schottky gate properties in the GaN/AlGaN HEMT structure. Figure 10 compares $I-V$ characteristics of the Pt/Au Schottky contacts with and without an Al-oxide interface layer fabricated on the NH_4OH-treated surface of GaN/AlGaN heterostructures. In the forward bias region, good linearity of the log $(I)-V$ relation was obtained for the contact with the Al-oxide interface layer. This contact showed relatively small ideality factor, n, of 1.17, similar to the normal Schottky contact. This means that the insertion of the Al-oxide layer did not disturb current transport based on the thermionic emission process. Significant improvement in the $I-V$ characteristics was seen in the reverse bias region, i.e., the reduction of reverse leakage current in about two orders of magnitude. This seems to be due to the formation of uniform ultrathin Al-oxide layer on the AlGaN surface.

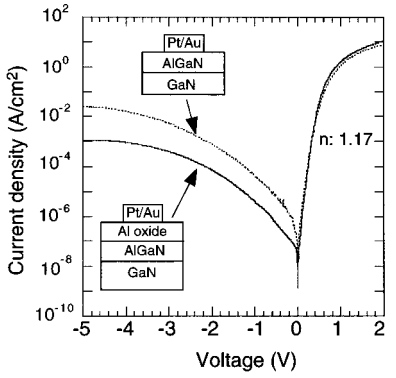

FIG. 10. $I-V$ characteristics of the Pt/Au Schottky contacts with and without an Al-oxide interface layer fabricated on the NH_4OH-treated surface of GaN/AlGaN heterostructures.

The Schottky gate controllability of 2DEG was evaluated by measuring $C-V$ characteristics.[29] Figure 11 shows the profiles of electron concentration near the GaN/AlGaN interface as a function of distance from the top AlGaN surface. The measured $C-V$ curves are shown in the inset of Fig. 11. A slight decrease in capacitance at zero bias is probably due to the insertion of the Al-oxide layer. The value of the capacitance change corresponded to the equivalent increase of the thickness of the AlGaN layer to be 1.5 nm. This is very close to nominal thickness of the Al-oxide layer when we assume the dielectric constant, ϵ_s, of the Al oxide (e.g., ϵ_s of $Al_2O_3=8.5$) is close to that of AlGaN ($\epsilon_s=9.0$). For the Al-oxide inserted contact, the pinch-off voltage is 0.3–0.4 V smaller than that of the normal contact, and steep onset behavior was seen in the $C-V$ curve.

As shown in the carrier profiles, the high electron concentration was observed at the AlGaN/GaN interface, similar to the results reported by Yu *et al.*[30] and Manfra *et al.*[31] This indicated the existence of 2DEG at the interface. Away from the heterointerface, the electron concentration falls off sharply and then saturates in the profile obtained from the Al-oxide inserted contact. This is consistent with the growth design, as shown in Fig. 1(c). On the other hand, the electron concentration gradually decreases even in the undoped GaN layer region for the profile obtained by the normal contact, as indicated by the broken line in Fig. 11. Steep increase of the leakage current (Fig. 10) seems to be one of possible reasons for such behavior. These results indicated that a surface passivation structure using an ultrathin Al-oxide layer is effective in improving the Schottky gate control of 2DEG in GaN/AlGaN HEMT structures.

IV. CONCLUSION

We have investigated chemical and electrical properties of surfaces of GaN and GaN/AlGaN heterostructures for the optimization of a surface passivation process. *In situ* XPS study revealed that relatively smaller band bending of 0.6 eV existed at the GaN (2×2) surface grown by rf–MBE on the MOVPE GaN template. The air-exposed sample showed strong band bending. The surface treatment in NH_4OH solution and ECR N_2 plasma was found to reduce the surface

Fermi level pinning. Surface passivation process of GaN utilizing SiN_x film prepared by the ECR–CVD achieved low interface state density, D_{it} of $2\times10^{11}\,cm^{-2}\,eV^{-1}$. The present NH_4OH/ECR–N_2 plasma treatment was also found to be effective in realizing well ordered and nearly oxide-free surface of a GaN/AlGaN heterostructure. The subsequent passivation process using the ECR–CVD SiN_x film enhanced the drain current in the gateless GaN/AlGaN HEMT. A surface passivation process utilizing an ultrathin Al-oxide layer reduced reverse leakage current and improved gate controllability of 2DEG in the Schottky gate contact fabricated on the GaN/AlGaN heterostructure. The present passivation processes are promising for realizing reproducibility of the device fabrication process and reliability of the device operation in GaN-based high-power/high-frequency devices.

ACKNOWLEDGMENTS

The authors thank M. Kihara of Hitachi Cable Ltd. for the supply of MOVPE GaN and GaN/AlGaN HEMT samples. This work was partly supported by a grant-in-aid for Scientific Research (B) (No. 11555081) and (C) (No. 11650309) from the Ministry of Science, Education, Sports, and Culture, Japan.

[1]U. Mishra, presented at the International Workshop on Nitride Semiconductors (IWN2000), 24–27 September 2000, Nagoya.
[2]B. M. Green, K. K. Chu, E. M. Chumbes, J. A. Smart, J. M. Shealy, and L. F. Eastman, IEEE Electron Device Lett. **21**, 268 (2000).
[3]S. L. Rumyantsev *et al.*, J. Appl. Phys. **88**, 6726 (2000).
[4]V. M. Bermudez, J. Appl. Phys. **80**, 1190 (1996).
[5]C. I. Wu and A. Kahn, J. Vac. Sci. Technol. B **16**, 2218 (1998).
[6]V. M. Bermudez, D. D. Koleske, and A. E. Wickenden, Appl. Surf. Sci. **126**, 69 (1998).
[7]H. C. Casey, Jr., G. G. Fountain, R. G. Alley, B. P. Keller, and S. P. DenBaars, Appl. Phys. Lett. **68**, (1996).
[8]M. Sawada, T. Sawada, Y. Yamagata, K. Imai, H. Kimura, M. Yoshino, K. Iizuka, and H. Tomozawa, J. Cryst. Growth **189/190**, 706 (1998).
[9]R. Therrien, G. Lucovsky, and R. Davis, Appl. Surf. Sci. **166**, 513 (2000).
[10]M. Hong *et al.*, J. Vac. Sci. Technol. B **18**, 1453 (2000).
[11]M. A. Kahn, X. Hu, G. Simin, A. Lunev, J. Yang, R. Gaska, and M. S. Shur, IEEE Electron Device Lett. **21**, 63 (2000).
[12]M. A. Kahn, X. Hu, A. Takakji, G. Simin, J. Yang, R. Gaska, and M. S. Shur, Appl. Phys. Lett. **77**, 1339 (2000).
[13]P. Hacke, G. Feuillet, H. Okumura, and S. Yoshida, J. Cryst. Growth **175/176**, 94 (1997).
[14]A. R. Smith, R. M. Feenstra, D. W. Greve, M.-S. Shin, M. Skowronski, J. Neugebauer, and J. E. Northrup, Appl. Phys. Lett. **72**, 2114 (1998).
[15]I. Waki, H. Fujioka, K. Ono, M. Oshima, H. Miki, and A. Fukizawa, Jpn. J. Appl. Phys., Part 1 **39**, 4451 (2000).
[16]Y.-J. Lin and C.-T. Lee, Appl. Phys. Lett. **77**, 3986 (2000).
[17]G. Hollinger, S. Skheyta-Kabbani, and M. Gendry, Phys. Rev. B **49**, 11159 (1994).
[18]N. J. Watkins, G. W. Wicks, and Y. Gao, Appl. Phys. Lett. **75**, 2602 (1999).
[19]J. R. Waldrop and R. W. Grant, Appl. Phys. Lett. **68**, 2879 (1996).
[20]C. I. Wu and A. Kahn, J. Appl. Phys. **86**, 3209 (1999).
[21]M. A. Kahn, J. N. Kuznia, D. T. Olson, and R. Kaplan, J. Appl. Phys. **73**, 3108 (1993).
[22]S. S. Dhesi, C. B. Stagarescu, K. E. Smith, D. Doppalapudi, R. Singh, and D. Moustakas, Phys. Rev. B **56**, 10271 (1997).
[23]K. Rapcewicz, M. B. Nardelli, and J. Bernholc, Phys. Rev. B **56**, R12725 (1997).
[24]A. R. Smith, R. M. Feenstra, D. W. Greve, J. Neugebauer, and J. E. Northrup, Phys. Rev. Lett. **79**, 3934 (1997).
[25]S. D. Wolter, J. M. DeLucca, S. E. Mohny, R. S. Kern, and C. P. Kuo, Thin Solid Films **371**, 153 (2000).
[26]T. Hashizume, S. Ootomo, R. Nakasaki, S. Oyama, and M. Kihara, Appl. Phys. Lett. **76**, 2880 (2000).
[27]M. K. Das, J. A. Cooper, Jr., and M. R. Melloch, J. Electron. Mater. **27**, 353 (1997).
[28]C.-M. Zetterling, M. Östling, K. Wongchotigul, M. G. Spencer, X. Tang, C. I. Harris, N. Nordell, and S. S. Wong, J. Appl. Phys. **82**, 2990 (1997).
[29]O. Ambacher *et al.*, J. Appl. Phys. **85**, 3222 (1999).
[30]E. T. Yu, G. J. Sullivan, P. M. Asbeck, S. D. Wang, D. Qiao, and S. S. Lau, Appl. Phys. Lett. **71**, 2794 (1997).
[31]M. J. Manfra, L. N. Pfeiffer, K. W. West, H. L. Stormer, K. W. Baldwin, J. W. P. Hsu, D. V. Lang, and R. J. Molnar, Appl. Phys. Lett. **77**, 2888 (2000).